Atom Manipulation Using Atomic Force Microscopy at Room Temperature

Y. Sugimoto, M. Abe and S. Morita

Abstract Atomic force microscopy (AFM) has demonstrated its capabilities as a nanotechnology tool. These capabilities include imaging/characterizing individual atoms on various surfaces and manipulating atoms and molecules. Here, we report how atom manipulation works on a well-known semiconducting surface, Si(111)-(7 × 7). To quantify the stochastic behavior of atom manipulation at room temperature (RT), atom hopping probabilities with various tip–surface distances are derived. The different hopping processes of Si adatoms have different tendencies in the probability plots. More remarkably, the ability of atom manipulation strongly depends on the AFM tip used. Tips can be characterized by their interaction force with surface Si adatoms. Force spectroscopic measurements combined with atom manipulation clarified that the ability to manipulate atoms is correlated with maximum attractive chemical bonding force with surface Si adatoms. Knowing the degree of chemical reactivity on the tip apex used for manipulation is key to enhancing the efficiency of the manipulation process occurring on semiconductor surfaces.

Keywords Atom manipulation · Non-contact atomic force microscopy · Force spectroscopy

Y. Sugimoto (✉)
Graduate School of Engineering, Osaka University, 2-1 Yamada-Oka, Suita, Osaka 565-0871, Japan
e-mail: sugimoto@afm.eei.eng.osaka-u.ac.jp

M. Abe
Graduate School of Engineering, Osaka University, 1-3 Machikaneyama-Cho, Toyonaka, Osaka 560-8531, Japan
e-mail: abe@stec.es.osaka-u.ac.jp

S. Morita
The Institute of Scientific and Industrial Research, Osaka University, 8-1 Mihogaoka, Ibaraki, Osaka 567-0047, Japan
e-mail: smorita@eei.eng.osaka-u.ac.jp

P. Moriarty and S. Gauthier (eds.), *Imaging and Manipulation of Adsorbates Using Dynamic Force Microscopy*, Advances in Atom and Single Molecule Machines,
DOI 10.1007/978-3-319-17401-3_3

1 Introduction

The ability to manipulate individual atoms on a surface is a remarkable feature of scanning probe microscopy [1]. Artificial nanostructures have been constructed for technological, physical, and chemical experiments using scanning tunneling microscopy (STM) at cryogenic temperatures [2–6]. Sophisticated atom positioning is usually controlled by the tiny force between the apex of the tip and the target atom on a surface [7].

Atomic force microscopy (AFM), the working principle of which is based on the detection of the tip–sample interaction force, has been developed as a versatile tool for imaging various surfaces, including insulator surfaces and organic molecular systems. The invention of a frequency modulation technique meant that atomic resolution could be routinely obtained [8]. The shift of frequency (Δf) from the resonance frequency (f_0) of an oscillated cantilever is detected for measurement of the tip–surface interaction force [9, 10]. One of the central analytical techniques in AFM is site-specific force spectroscopy measuring Δf with the tip–surface distance [i.e., $\Delta f(z)$]. The interaction force between the atoms of the tip apex and individual surface atoms can be quantified by conversion from $\Delta f(z)$. Since the first demonstration of quantification of a single chemical bonding force on the Si(111)-(7 × 7) surface [11], various applications have used force spectroscopy with atomic resolution, including chemical identification by maximum attractive covalent bonding force [12, 13], direct estimation of magnetic exchange force [14, 15], and clarification of the fundamental relationship between current and chemical force [16, 17]. Extension of the dimensionality of the measured force field has been also developed. One can obtain a 3D force map by acquiring Δf data in the volume on surfaces and converting it to a force map. There are many reports of force mapping measured on metal surfaces [18, 19], semiconductor surfaces [20–22], insulator surfaces [23–27], and molecules [28–33]. AFM has evolved from a surface imaging tool to a mapping tool for visualization of the force field on surfaces.

In addition to imaging and force spectroscopy, we have demonstrated that atom manipulation can be performed using AFM at large cantilever oscillation amplitudes [34–40]. Our first study of mechanical vertical manipulation using AFM was reported in 2003 [34]. We demonstrated that single Si adatoms can be extracted from the Si(111) surface reproducibly at low temperature (LT). Such vertical atom extraction is illustrated in Fig. 1a. A demonstration of lateral atom manipulation on a Ge surface at LT was published in 2005 [35]. Lateral manipulation means that single atoms residing on a surface are manipulated laterally (see Fig. 1d). Shortly, thereafter, we showed atom manipulation and assembly at room temperature (RT). This AFM manipulation achieved precision similar to that reported in LT manipulation using STM [36]. To avoid thermal diffusion at RT, we used a novel technique, called interchange lateral atom manipulation. In this method, the positions of two different elements are exchanged in the plane of a semiconducting alloy surface, as shown in Fig. 1e. In 2008, we discovered yet another interchange manipulation, called interchange vertical atom manipulation [38]. In this new

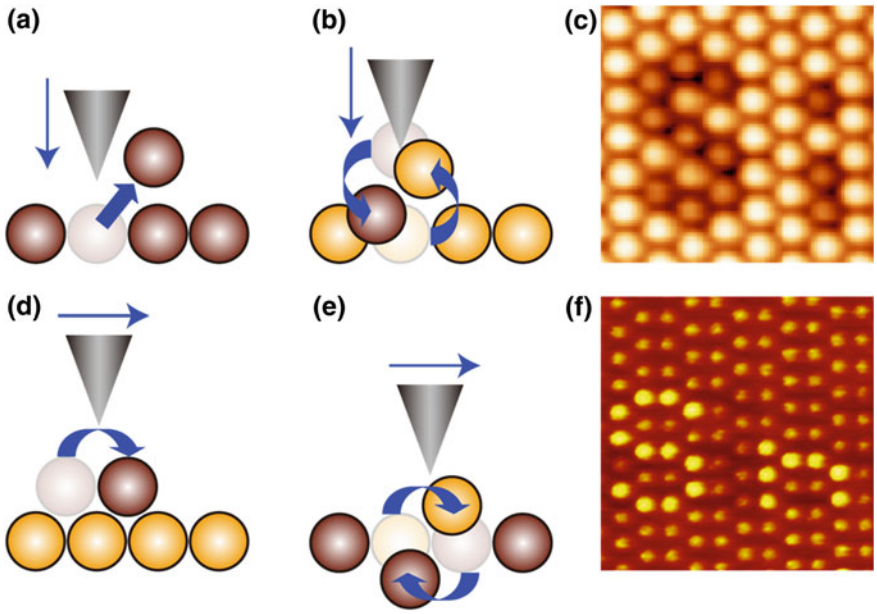

Fig. 1 Four different types of atom manipulation and atom letters. **a** Illustration of vertical atom manipulation; **b** interchange vertical atom manipulation; **d** lateral atom manipulation; and **e** interchange lateral atom manipulation. **c** The symbol 'Si' assembled by interchange vertical manipulation at RT [38], and **f** the symbol 'Sn' assembled by interchange lateral manipulation at RT [36]

vertical manipulation, atoms on the tip apex are vertically exchanged with surface atoms as shown in Fig. 1b. This process is reproducible enough to engineer nanostructures on surfaces at RT. Interchange vertical/lateral atom manipulation allows us to construct planer nanostructures by rearranging two different adatom species on semiconductor surfaces at RT, as shown in Fig. 1c, f, respectively [36, 38]. These techniques at RT are highly promising for atom-by-atom construction of nanodevices able to operate in ambient conditions.

Moreover, using AFM, it is possible to investigate the interaction force associated with mechanical atom/molecule manipulation [18, 37, 38, 41–43]. Ternes et al. [18] measured the force required to move a metal adsorbate on a metallic surface using a quartz cantilever oscillated at sub-angstrom amplitude. Lateral manipulation of metal adsorbates is dominated by the lateral force only, independent of the vertical force. This result is in contrast to manipulation mechanisms proposed on the semiconducting surface where the vertical force plays an important role in atom movement by reducing the energy barrier [37]. The relation between mechanical atom manipulation and measured tip–surface interaction force, as well as the role played by the tip, is still open questions.

In this study, we combine the capability of AFM to manipulate single atoms at RT with force measurement techniques. The relation between tip reactivity and ability of the tip to move atoms is systematically investigated on the Si(111)-(7 × 7) surface.

2 Experimental Procedure

We used an ultrahigh vacuum AFM operated at RT. Commercial Si cantilevers with first resonant frequency of the order of 100 kHz were used. The tip apex was cleaned with an Ar ion sputtering in an ultrahigh vacuum. A homebuilt interferometer was used to detect the cantilever deflection, as shown schematically in Fig. 2. Note that a cantilever deflection sensor based on the optical interferometer enabled us to measure the tip–sample interaction force with high sensitivity [44]. In addition, decoupling of the force and tunneling current signals were guaranteed, which is essential for reliable simultaneous AFM/STM measurements [17, 22, 45–47].

Control of cantilever oscillation with constant amplitude and frequency measurements was performed using PLL-based commercial electronics. Cantilevers with a typical spring constant of 10–50 N/m were oscillated at a 10 nm order of oscillation amplitude to avoid jump into contact [48]. The tip–surface distance was regulated by feedback of the shift in the cantilever's first mechanical resonant frequency to the distance piezo. A commercial digital scanning controller was used for AFM scanning, force spectroscopic experiments, and atom manipulation experiments [49].

We used Si(111) samples of cut Si wafer for our atom manipulation and force spectroscopy experiments. The Si(111)-(7 × 7) surface was obtained by direct-current heating with vacuum pressure kept below 1×10^{-10} Torr. The sample was flashed up to 1200 °C, followed by annealing.

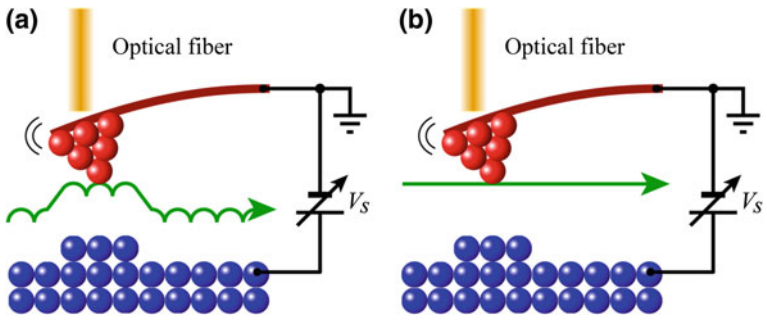

Fig. 2 Schematic views of our cantilever-based AFM setup: **a** topographic scan mode; and **b** constant height scan mode

3 Manipulation of Si Atoms at Room Temperature

Although precise atom assembly was realized even at RT by the interchange lateral/vertical atom manipulation method, the manipulation mechanism on semiconducting surfaces at RT was not clear. Since the atom exchange process is complicated, we began by investigating lateral movement of the surface Si adatoms on the Si(111)-(7 × 7) surface by tip interaction. It was challenging to laterally manipulate single atoms that adsorbed on the surfaces at RT because of unwanted thermal diffusion. We found, however, that Si adatoms could be laterally manipulated toward a vacancy of adatom with high precision, even at RT [37, 39, 50]. Such vacant adatom positions were used as an open space toward which Si adatoms were manipulated.

Several AFM images of the same location on the Si surface are shown in Fig. 3a–h, which demonstrates manipulation of Si adatoms. The gray arrow in Fig. 3a indicates the vacancy created by vertical manipulation to supply a marker. An Si adatom vacancy was created by the mechanical atom extraction technique [34]. The procedure for this is given as follows. First, we scanned the Si(111)-(7 × 7) surface by AFM and selected a surface region that was suitable for atom manipulation experiments near the center of a terrace. The AFM scan was then stopped, and the tip was positioned over the Si adatom to be removed. After the feedback for the regulation of the tip–surface distance was deactivated, the tip approached the surface by a certain small displacement and then retracted to the original height. The feedback loop was then reactivated, and an AFM scan was carried out to check that atom extraction had been successful. The controlled indentation procedure was repeated with gradual increments of displacement until a Si adatom vacancy was successfully created. If the tip state became unstable after atom extraction, the tip was laterally moved to a different surface area, typically 10 nm away from the created vacancy site, and changed by intentional tip–surface contact or by AFM scanning under close tip–surface distances until the tip state was stabilized. When clear atomic resolution was obtained and the tip state was stable such that no further tip changes occurred during scanning, even under close tip–surface distances, the tip was brought to the area where the vacancy was created and an AFM topographic image was obtained over this region.

The white triangles in the images of Fig. 3a–h show an equivalent faulted half-unit cell, including the second vacancy created. In this triangle, Si adatoms were manipulated. The lateral manipulation of Si adatoms resulted in a change in the vacancy position, imaged as dark. The Si adatoms were manipulated along the dimer rows (along the sides of a triangle) in Fig. 3a–f. The atom could be also manipulated across the half-unit cell, as shown in Fig. 3f–h. In this manipulation, we were able to put a Si adatom on an unusual adsorption site (called an M site). An Si adatom adsorbed on the M site stably, such that the Si atom could be imaged by AFM within the experimental timescale under a weak tip–surface interaction. Figure 3g shows the AFM image of the artificial configuration. The vacancy is split, and three Si adatoms align horizontally in the half-unit cell. The atom configuration

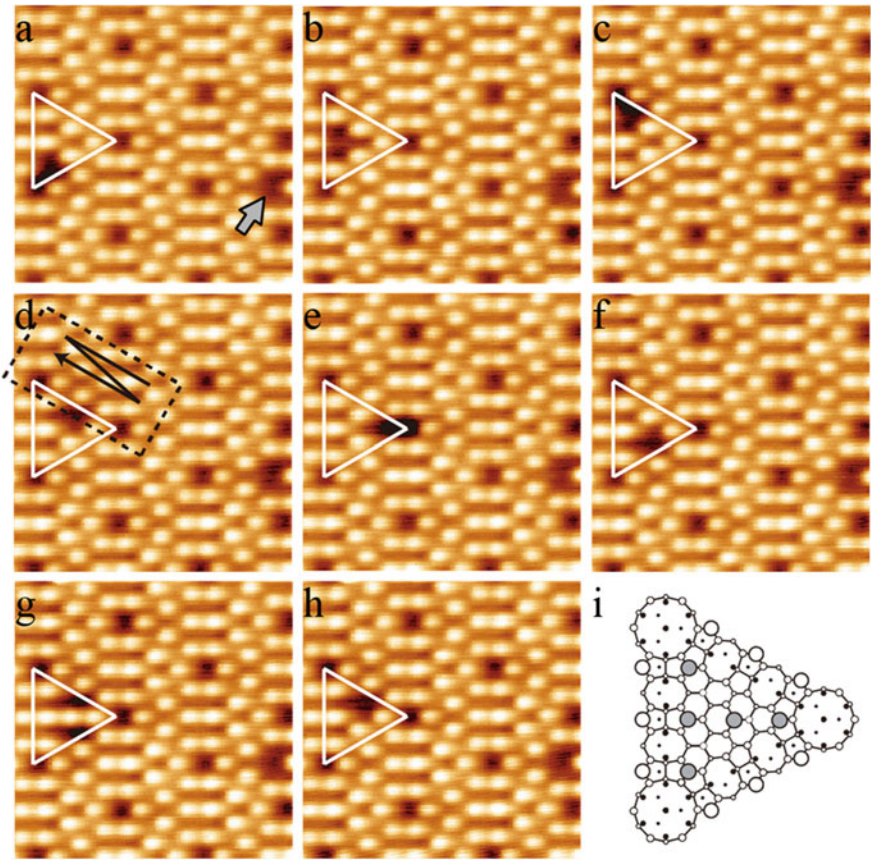

Fig. 3 **a**–**h** AFM topographic images showing lateral manipulations of Si adatoms on the Si(111)-(7 × 7) [37]. The *gray arrow* in **a** indicates a missing adatom vacancy created by vertical manipulation for a marker. The acquisition parameters are f_0 = 162,295.8 Hz, A = 282 Å, and k = 28.7 N/m. Frequency shift set points for imaging (Δf_{image}) and manipulation (Δf_{move}) were −3.9 and −5.1 Hz, respectively. Si adatom can be put into an unusual metastable site, as shown in **i**, which is a stick and ball model that displays the atomic configuration

of this artificial structure is schematically illustrated in Fig. 3i. The manipulated Si adatom sits in a T_4 site near the center of the half-unit cell and forms bonds to an original surface rest atom.

These manipulations were performed using a vector scanning method in which the tip–sample distance feedback was closed, i.e., the topographic mode (see Fig. 2a). The procedure performed between Fig. 3d and e is shown in Fig. 3d. A Si adatom on a corner site (Co) was laterally manipulated to a center adatom site (Ce) by the method described below. After the initial image (Fig. 3d) was acquired, the scan area was reduced and the scan angle was rotated, as shown by the dotted rectangle. By the rotation of the scan angle, the fast scan direction coincided with

the line above the Si adatom to be manipulated and the vacancy. The fast scan direction was set to be one way, indicated by the black arrow, and the slow scan started from the top right of the dotted rectangle. When the slow scan line reached the line that included the vacancy, it was stopped and scanning on the same line was repeated. The Δf set point was then increased to be more negative, and the averaged tip–surface distance during line scans was decreased. Under a certain threshold distance, the Si adatom was manipulated toward the vacancy. After the signature of the atom movement appeared in the topographic signal, the averaged tip–surface distance was restored by setting the Δf set point to the original value. The final image shown in Fig. 3e indicated that the Si atom had been successfully manipulated toward the vacancy.

These manipulations were categorized into the pulling mode. Si adatoms were moved by the attractive force (negative Δf). First principle calculations [37] shed light on the details of the mechanism. The chemical interaction force reduces the potential energy barrier, resulting in a thermal hop of the adatom toward an adjacent vacancy site. In contrast to typical lateral manipulation on metal surfaces [18], the vertical force plays a role in manipulation in our Si system. The tip pulls the target Si adatom up by the vertical component of the attractive force. Due to the vertical relaxation of Si adatoms, the bonds with the backbond atoms are weakened, which contributes to the barrier reduction. We believe that the proposed interpretation is characteristic of semiconductor surfaces.

4 Relationship Between Atom Manipulation and the Measured Force

To further quantify the manipulation process and investigate the effect of the reactivity of the tip apex on the manipulation, we combined force spectroscopy and constant height manipulation using the same tips. Before the lateral atom manipulation on the Si(111)-(7 × 7) surface, force spectroscopic measurements were carried out to characterize tip apex reactivity. We applied atom tracking to position the tip just above the adatom for site-specific force spectroscopy [51]. For quantitative atom manipulation experiments, it is necessary to precisely adjust the scan line just above the vacancy and the manipulated adatoms. To accomplish this at RT, the tip was first positioned above another Si adatom that was also above the line but in a different half-unit cell by atom tracking. After measurement of the drift velocity during atom tracking, thermal drift was compensated by the feedforward controller [20]. Successive line scans were then carried out above the vacancy and the manipulated Si adatoms in the [1 −1 0] direction (the left-right arrow), as illustrated in Fig. 4a. The scan direction was precisely aligned parallel to the [1 −1 0] direction by a versatile scan controller [49]. More importantly, the tip was scanned at constant heights by switching off the feedback control for the tip–surface distance to make statistics at each tip–surface distance. During constant height scanning, the

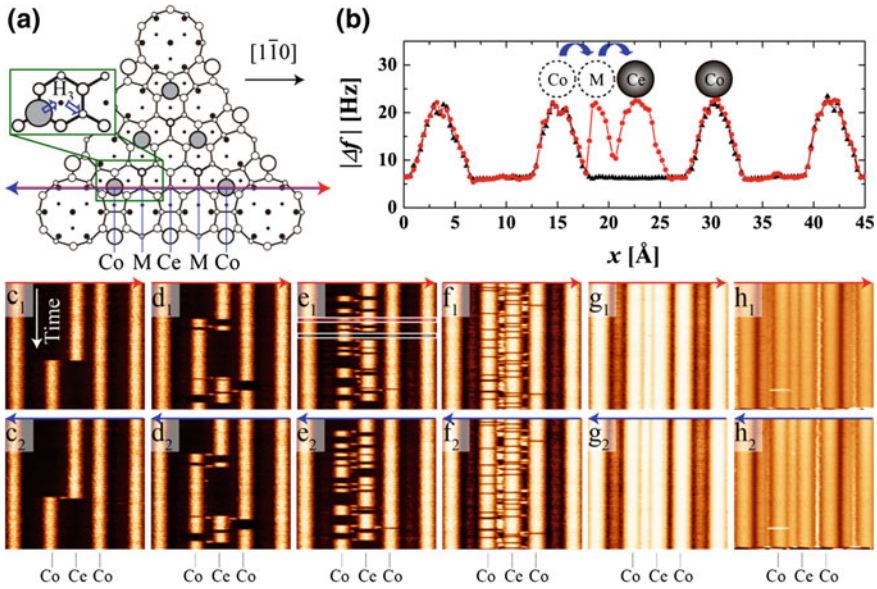

Fig. 4 Quantitative manipulation of Si adatoms at RT [50]. **a** A ball and stick model of a half-unit cell in the Si(111)-(7 × 7) surface. Single vacancy is illustrated on a Ce site. The theoretically found atom hopping path (Co → H_3 → M) is shown in the *rectangle*. The *horizontal left* and *right arrows* indicate the direction of the vector tip scanning for manipulation at constant height. The tip was successively scanned above the line of the *arrows*, connecting a vacancy and manipulated adatoms. **b** Two selected line profiles of Δf images from the constant height scan. $\mathbf{c_1}$–$\mathbf{h_2}$ Constant height Δf images at different tip–sample distances. The fast scan direction is from *left* to *right* ($\mathbf{c_1}$–$\mathbf{h_1}$) and *right* to *left* ($\mathbf{c_2}$–$\mathbf{h_2}$). Corresponding distances for the Δf images: $\mathbf{c_1}$, $\mathbf{c_2}$ z = 0.21 Å; $\mathbf{d_1}$, $\mathbf{d_2}$ z = 0.12 Å; $\mathbf{e_1}$, $\mathbf{e_2}$ z = 0.02 Å; $\mathbf{f_1}$, $\mathbf{f_2}$ z = −0.17 Å; $\mathbf{g_1}$, $\mathbf{g_2}$ z = −0.31 Å; and $\mathbf{h_1}$, $\mathbf{h_2}$ z = −1.16 Å. Here, the z values were defined from the force curves in Fig. 5a; i.e., z = 0 corresponding to maximum attractive force. Both line profiles in **b** were extracted from $\mathbf{e_1}$ and so were acquired with the same parameters. The profile with symbols of *black triangles* does not show the signature atom hopping. On the other hand, in the profile with *red circles*, we can see the signature atom hop from a *left* Co site to an M site, followed by a successive jump to a Ce site

Δf signal was recorded (see Fig. 2b). This scanning mode is indispensable for reducing the risk of a tip crash during atom manipulation. The slope of the Δf (z) curves above the adatom sites changes the polarity at the tip–surface distances where atom hopping probability is large, because the long-range force is relatively small for sharp Si tips.

Figure 4c_1–h_2 shows the Δf images of the constant height line scans on the Si (111)-(7 × 7) surface. The horizontal arrows in Fig. 4a indicate the scan line. Each image in Fig. 4c_1–h_2 shows the Δf signal at a constant height vector scan, so the bright stripes correspond to individual Si adatoms. Discontinuity and intermittent patterns reflect atom hopping processes caused by interaction with the tip. The fast scan direction from left to right is shown in (c_1–h_1) and right to left is shown in (c_2–h_2). All images in Fig. 4 were acquired using the same tip. From (c_1, c_2) to (h_1, h_2), the

tip–surface distance decreased: Δf images in c_1 and c_2 were measured at a far tip–surface distance, while those in h_1 and h_2 were measured at the closest tip–surface distance.

The Si adatoms were moved following the tip scan when the tip–surface distance became small. From the Δf images, we can see which adsorption sites were occupied by the Si adatoms, so atom movement could be followed. The atom manipulation process is stochastic at RT. Different manipulation processes could be observed in line profiles of Δf images even at the same scan parameter of the tip–sample distance [39]. For example, two different line profiles are shown in Fig. 4b. These line profiles were taken from the Δf image as shown in Fig. 4e_1. The line profile with the black triangles shows that two Si adatoms stay at left and right Co sites without any atom movement. In contrast, the line profile with the red circles shows the signature of atom displacement. Initial atom configuration is the same between the two profiles. The latter profile demonstrates atom hopping as follows. When the tip scans from the left, the left Co adatom is imaged. At x = 17.8 Å, the Si adatom is moved to the M site following the tip, causing the Δf jump. When the tip reaches x = 20.7 Å, the same Si adatom jumps to the Ce site. There was a vacancy at the Ce site before this manipulation, while the vacancy appears on the left Co site after the scan.

Figure 4b shows that the manipulation process is stochastic at RT. To quantify the probability of successful manipulation, we analyzed a number of Δf images measured at various tip–surface distances. We calculated the probability as the number of line profiles showing particular manipulation processes divided by the number of total line profiles. The results obtained at a certain tip state are shown in Fig. 5a. Three different probability plots are shown as a function of the tip–surface distance. Solid (open) circles show the probabilities of atom hops from left (right) Co to M sites, and open triangles show the probabilities of hops from Ce to M sites. In Fig. 5a, the chemical bonding force [$F_z(z)$] and chemical bonding potential [$U(z)$] are shown together. Those curves were numerically converted from the measured $\Delta f(z)$ curve above the Si adatom by the same tip state used for manipulation experiments. The tip approach increases the probability of atom hopping for all three processes. This increase was not step-like as expected at absolute zero temperature. Around the maximum $F_z(z)$, the probabilities smoothly increase from 0 to 100 %, which is a feature of manipulation at RT.

Most remarkably, the success rate of the manipulation strongly depended on the tip apex state. To systematically investigate the tip dependence of the manipulation, we carried out the same experiments with 15 different tips using 10 different cantilevers. Different tip states for the same cantilever were prepared by controlled tip crash to the surface. In our extended studies, two kinds of tips were found, i.e., the tips that could move atoms and those that could not. Figure 5a is an example of the former group, while Fig. 5b is an example of the latter. The probability of atom movement remains zero even for tip–surface distances closer than the distance of maximum attractive force. Interestingly, the tip state that does not have manipulation capability can be changed. After the intentional tip change, the results shown in Fig. 5c were obtained. This tip state has the ability of atom manipulation. All

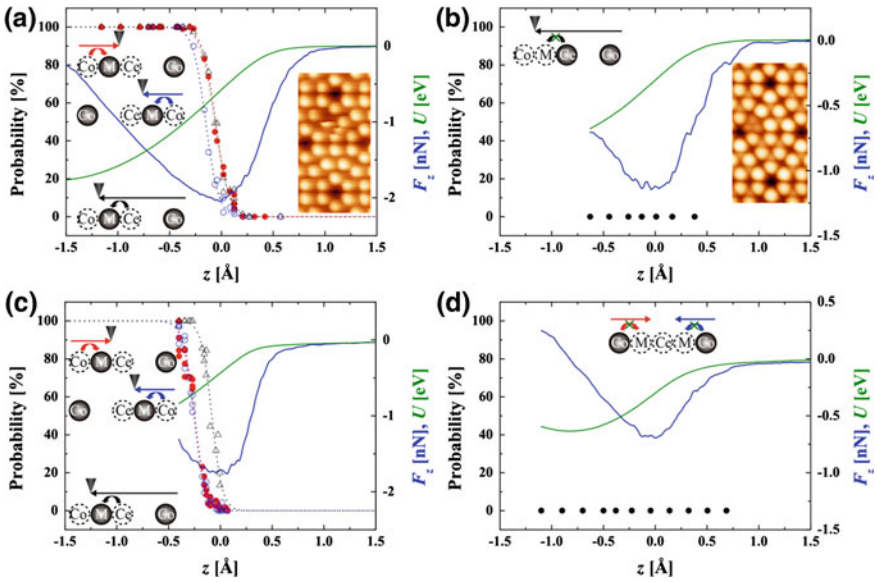

Fig. 5 Hopping probability plots with $F_z(z)$ and $U(z)$ curves. Results with four different tips are shown [50]. **a** *Solid circles* correspond to the probability of the atom hopping from the left Co to the M site. *Open circles* correspond to the likelihood of the atom hopping from the right Co to the M site. *Open triangle* shows Ce to the M site. **b** This data do not show atom manipulation. **c** The data set acquired by using the same cantilever as in **b**, but with a different tip state. The different tip state is prepared by a gentle tip–surface crash. Assignment of the symbols for the manipulation process is the same as in **a**. **d** These data do not show atom manipulation. The *insets* of **a** and **b** show corresponding AFM topographic images

processes observed in Fig. 5a were reproduced in Fig. 5c. The different tendencies of the manipulation between Fig. 5a and c will be discussed later. Figure 5d shows the result with a different tip state and different cantilever from those used in Figs. 5a–c. In Fig. 5d, the Si adatoms cannot be moved in either the forward or backward scan direction even at distances where F_z on Si adatom reaches the repulsive force region. These results clearly show that the properties of the few atoms at the very apex of the tip are essential to manipulation.

We found that manipulation capability can be characterized by the interaction force with surface adatoms. Figure 6a displays a histogram of magnitude of the maximum attractive force F_{max} of 15 different tips. The forces were measured above the Si adatom. In the graph, it is clear that manipulation capability is significantly correlated with F_{max}. Thus, F_{max} can be used to categorize the 15 tips measured into two groups. The group with larger F_{max} has the capability to manipulate Si adatoms, while it is not possible to move atoms using the group with the smaller F_{max}. We call the tips with larger F_{max} reactive tips and the others less-reactive tips. To manipulate Si adatoms as shown in Fig. 3, reactive tips are necessary.

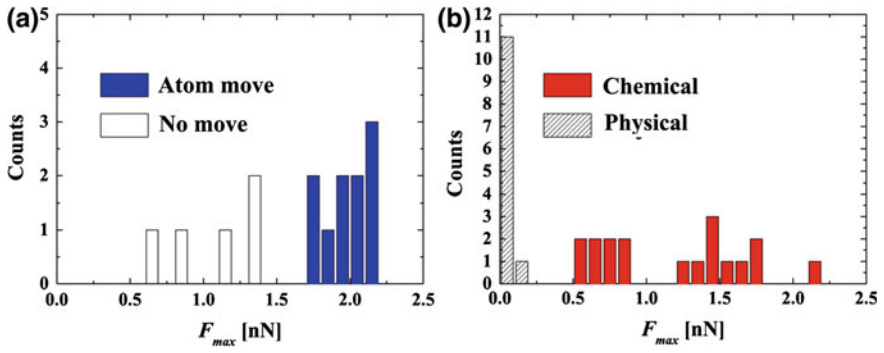

Fig. 6 **a** The histogram of the maximum attractive forces with 15 different tips [50]. The forces were acquired by force spectroscopy above Si adatoms. There are two groups. The tips with larger attractive force can move atoms. The other tips with smaller force cannot move atoms even at close tip–surface distances. **b** The histogram of maximum attractive short-range forces measured above Si adatoms besides atom manipulation experiments. There is a group showing tiny F_{max}, i.e., physical force [52]

These two types of tips can be identified from AFM images with relatively close tip–surface distances. With a reactive tip, during AFM scanning, one will be able to observe that Si adatoms are moved following the tip (see the inset image in Fig. 5a). In contrast, with a less-reactive tip, one will obtain an AFM image without fluctuation around the vacancy site. In Fig. 5b, even Si rest atoms can be clearly resolved.

It is worth nothing that there is a third class of tip apex, i.e., the non-reactive tip. Non-reactive tips cannot provide clear atomic resolution on the Si(111)-(7 × 7) surfaces by AFM (as opposed to all the tips in Fig. 6a that gave a clear atomic resolution). In addition to the atom manipulation experiments shown in Fig. 6a, we measured F_{max} on Si adatoms on the Si(111)-(7 × 7) surfaces using various tips. As shown in the histogram of Fig. 6b, the tips that cannot provide atomic resolution have extremely small F_{max}, usually less than 0.1 nN [52]. The other tips giving atomic resolution have F_{max} larger than 0.5 nN, and the dispersion of F_{max} is the same as that in Fig. 6a.

Thus, it is possible to manipulate Si adatoms with reactive tips. More specifically, we can discuss the anisotropy of the manipulation direction depending on the tip. Direction can be investigated by equivalent manipulation processes from the Co to the M site, but in opposite scan directions. In Fig. 5a, solid (open) circles indicate the probability plots from the left (right) Co site to the M site. Although those processes are equivalent, the probability plots differ with the scan directions. The probability from left to right starts to increase at farther distances than that from right to left. This is likely due to a tip asymmetry effect. Asymmetric tip structures may also produce asymmetric dangling bond states with respect to the surface. Recently, Jarvis et al. [53] reported theoretical studies about tip effects on vertical manipulation. The manipulation depended on the orientation of the dangling bond.

Therefore, we can assume that the tip had an asymmetric structure in Fig. 5a. Symmetric results can be also obtained, as shown in Fig. 5c. There, the probability plots for different tip scans match. Such a tip may have symmetric structure with respect to scan direction.

Finally, we should note that correlation between the capability of atom manipulation and F_{max} was reproduced by first principle calculations [50]. The energy barrier for Si adatom under the interaction with the tip was calculated. Tips with different degrees of reactivity decreased the energy barrier differently. The tip that interacts with surface Si adatoms strongly can reduce the barrier more. Therefore, the theoretical studies reproduce our results; that is, only a reactive tip can manipulate Si adatoms on the Si(111)-(7 × 7) surface.

5 Conclusions

We performed force spectroscopic measurements on Si adatoms on Si(111)-(7 × 7) surfaces using various tips of AFM. It was found that tips could be categorized into three groups: non-reactive, less reactive, and more reactive. Non-reactive tips interact with the adatom by physical force, and atomic resolution cannot be clearly obtained on the surface by AFM. The other two groups can give clear atomic resolution by chemical interaction force. Using the latter two classes of tips, we systematically investigated the relation between degree of reactivity on AFM tip and capability of lateral manipulation on the Si(111)-(7 × 7) surface at RT. It was found that the less-reactive tips did not have the capability of atom manipulation, while the more-reactive tips did. We found clear correlation between the capability of the manipulation and the degree of tip reactivity that can be characterized by the magnitude of the maximum attractive force with surface Si adatoms. This may be related to the 'sticky fingers problem' pointed out by Smalley [54]. For efficient manipulation, one should tune the extent of the chemical reactivity with the interaction strength between manipulated atom and substrate in mind. Once a suitable tip is obtained, it will be possible to manipulate atoms at will—even on reactive semiconducting surfaces—by adjusting the tip–surface interaction through the distance control.

Acknowledgments This work was supported by a grant-in-aid for Scientific Research from MEXT, Funding Program for Next Generation World-Leading Researchers. I would like to thank my colleagues who contributed to this study: Ayhan Yurtsever, Oscar Custance, Martin Ondracek, Pavel Jelinek, Pablo Pou, and Ruben Perez.

References

1. Eigler, D.M., Lutz, C.P., Rudge, W.E.: Nature (London) **352**, 600 (1991)
2. Nilius, N., Wallis, T.M., Ho, W.: Science **297**, 1853–1856 (2002)
3. Heinrich, A.J., Lutz, C.P., Gupta, J.A., Eigler, D.M.: Science **298**, 1381 (2002)

4. Hla, S.W., Braun, K.F., Rieder, K.H.: Phys. Rev. B **67**, 201402 (2003)
5. Loth, S., Baumann, S., Lutz, C.P., Eigler, D.M., Heinrich, A.J.: Science **335**, 196–199 (2012)
6. Khajetoorians, A.A., et al.: Science **339**, 55–59 (2013)
7. Bartels, L., Meyer, G., Rieder, K.-H.: Phys. Rev. Lett. **79**, 697 (1997)
8. Albrecht, T.R., Grütter, P., Horne, D., Rugar, D.: J. Appl. Phys. **69**, 668–673 (1991)
9. Morita, S., Wiesendanger, R., Meyer, E. (eds.): Noncontact Atomic Force Microscopy. Springer, Berlin (2002)
10. Giessibl, F.J.: Rev. Mod. Phys. **75**, 949–983 (2003)
11. Lantz, M.A., et al.: Science **291**, 2580–2583 (2001)
12. Sugimoto, Y., et al.: Nature (London) **446**, 64–67 (2007)
13. Setvin, M., et al.: ACS Nano **6**, 6969–6976 (2012)
14. Schmidt, R., et al.: Phys. Rev. Lett. **106**, 257202 (2011)
15. Pielmeier, F., Giessibl, F.J.: Phys. Rev. Lett. **110**, 266101 (2013)
16. Ternes, M., et al.: Phys. Rev. Lett. **106**, 016802 (2011)
17. Sugimoto, Y., et al.: Phys. Rev. Lett. **111**, 106803 (2013)
18. Ternes, M., Lutz, C.P., Hirjibehedin, C.F., Giessibl, F.J., Heinrich, A.J.: Science **319**, 1066–1069 (2008)
19. Albers, B.J., et al.: Nat. Nanotechnol. **4**, 307 (2009)
20. Abe, M., et al.: Appl. Phys. Lett. **90**, 203103 (2007)
21. Sugimoto, Y., Namikawa, T., Miki, K., Abe, M., Morita, S.: Phys. Rev. B **77**, 195424 (2008)
22. Sugimoto, Y., Ueda, K., Abe, M., Morita, S.: J. Phys.: Condens. Matter **24**, 084008 (2012)
23. Holscher, H., Langkat, S.M., Schwarz, A., Wiesendanger, R.: Appl. Phys. Lett. **81**, 4428 (2002)
24. Schirmeisen, A., Weiner, D., Fuchs, H.: Phys. Rev. Lett. **97**, 136101 (2006)
25. Ruschmeier, K., Schirmeisen, A., Hoffmann, R.: Phys. Rev. Lett. **101**, 156102 (2008)
26. Kawai, S., Glatzel, T., Koch, S., Baratoff, A., Meyer, E.: Phys. Rev. B **83**, 035421 (2011)
27. Rahe, P., et al.: Rev. Sci. Instrum. **82**, 063704 (2011)
28. Ashino, M., Schwarz, A., Behnke, T., Wiesendanger, R.: Phys. Rev. Lett. **93**, 136101 (2004)
29. Ashino, M., et al.: Nat. Nanotechnol. **3**, 337 (2008)
30. Gross, L., Mohn, F., Moll, N., Liljeroth, P., Meyer, G.: *Science* **325**, 1110–1114 (2009)
31. Braun, D.A., Weiner, D., Such, B., Fuchs, H., Schirmeisen, A.: Nanotechnology **20**, 264004 (2009)
32. Sun, Z., Boneschanscher, M.P., Swart, I., Vanmaekelbergh, D., Liljeroth, P.: Phys. Rev. Lett. **106**, 046104 (2011)
33. Mohn, F., Gross, L., Meyer, G.: Appl. Phys. Lett. **99**, 053106 (2011)
34. Oyabu, N., Custance, O., Yi, I., Sugawara, Y., Morita, S.: Phys. Rev. Lett. **90**, 176102 (2003)
35. Oyabu, N., Sugimoto, Y., Abe, M., Custance, O., Morita, S.: Nanotechnology **16**, S112 (2005)
36. Sugimoto, Y., et al.: Nat. Mater. **4**, 156–159 (2005)
37. Sugimoto, Y., et al.: Phys. Rev. Lett. **98**, 106104 (2007)
38. Sugimoto, Y., et al.: Science **322**, 413–417 (2008)
39. Sugimoto, Y., Miki, K., Abe, M., Morita, S.: Phys. Rev. B **78**, 205305 (2008)
40. Sugimoto, Y., Yurtsever, A., Hirayama, N., Abe, M., Morita, S.: Nat. Commun. **5**, 4360 (2014)
41. Sweetman, A., et al.: Phys. Rev. Lett. **106**, 136101 (2011)
42. Mao, H.Q., Li, N., Chen, X., Xue, Q.K.: J. Phys.: Condens. Matter **24**, 084004 (2012)
43. Langewisch, G., Falter, J., Fuchs, H., Schirmeisen, A.: Phys. Rev. Lett. **110**, 036101 (2013)
44. Morita, K., Sugimoto, Y., Sasagawa, Y., Abe, M., Morita, S.: Nanotechnology **21**, 305704 (2010)
45. Sawada, D., Sugimoto, Y., Morita, K., Abe, M., Morita, S.: Appl. Phys. Lett. **94**, 173117 (2009)
46. Sugimoto, Y., Yi, I., Morita, K., Abe, M., Morita, S.: Appl. Phys. Lett. **96**, 263114 (2010)
47. Sugimoto, Y., et al.: Phys. Rev. B **81**, 245322 (2010)
48. Giessibl, F.J., Hembacher, S., Herz, M., Schiller, C., Mannhart, J.: Nanotechnology **15**, S79 (2004)

49. Horcas, I., et al.: Rev. Sci. Instrum. **78**, 013705 (2007)
50. Sugimoto, Y., et al.: ACS Nano **7**, 7370–7376 (2013)
51. Abe, M., Sugimoto, Y., Custance, O., Morita, S.: Appl. Phys. Lett. **87**, 173503 (2005)
52. Yurtsever, A., et al.: Phys. Rev. B **87**, 155403 (2013)
53. Jarvis, S., Sweetman, A., Bamidele, J., Kantorovich, L., Moriarty, P.: Phys. Rev. B **85**, 235305 (2012)
54. Smalley, R.E.: Sci. Am. **285**, 76 (2001)